Investigational New Drugs (2022) 40:905–921
https://doi.org/10.1007/s10637-022-01266-y

RESEARCH

Two novel piperidones induce apoptosis and antiproliferative effects on human prostate and lymphoma cancer cell lines

Risa Mia Swain[1] · Lisett Contreras[1] · Armando Varela-Ramirez[1] · Mohammad Hossain[3] · Umashankar Das[2] · Carlos A. Valenzuela[1] · Manuel L. Penichet[4] · Jonathan R. Dimmock[2] · Renato J Aguilera[1]

Received: 30 March 2022 / Accepted: 1 June 2022 / Published online: 6 July 2022

Summary
Cancer remains the second most common cause of death in the US. Due to a recurrent problem with anticancer drug resistance, there is a current need for anticancer drugs with distinct modes of action for combination drug therapy We have tested two novel piperidone compounds, named 2608 (1-dichloroacetyl – 3,5-bis(3,4-difluorobenzylidene)-4-piperidone) and 2610 (1-dichloroacetyl-3,5-bis(3,4-dichlorobenzylidene)-4-piperidone), for their potential cytotoxicity on numerous human cancer cell lines. We found that both compounds were cytotoxic for breast, pancreatic, leukemia, lymphoma, colon, and fibroblast cell lines, with a cytotoxic concentration 50% (CC_{50}) in the low micromolar to nanomolar concentration range. Further assays focused primarily on an acute lymphoblastic lymphoma and colon cancer cell lines since they were the most sensitive and resistant to the experimental piperidones. The cell death mechanism was evaluated through assays commonly used to detect the induction of apoptosis. These assays revealed that both 2608 and 2610 induced reactive oxygen species (ROS) accumulation, mitochondrial depolarization, and activated caspase-3/7. Our findings suggest that the piperidones induced cell death *via* the intrinsic apoptotic pathway. Additional assays revealed that both piperidones cause cell cycle alteration in lymphoma and colon cell lines. Both piperidones elicited DNA fragmentation, as evidenced by an increment in the sub-G0/G1 subpopulation in both cell lines. Similar to other related compounds, both piperidones were found to act as proteasome inhibitors by increasing the levels of poly-ubiquitinated proteins in both lymphoma and colon cell lines. Hence, the two piperidones exhibited attractive cytotoxic properties and suitable mechanisms of action, which makes them good candidates as anticancer drugs.

Keywords Colorectal Cancer · Hematopoietic malignancies · Cytotoxicity · Piperidones · Apoptosis · Anticancer · Dichloroacetate

Introduction

Cancer is caused by uncontrolled cell growth in the body that, if not curtailed, can lead to death [1]. An estimated 184,130 combined cases in the United States are expected to be diagnosed with leukemia, lymphoma, or multiple myeloma in 2022 [2]. Individuals with the highest risk for developing leukemia or lymphoma are children of Hispanic heritage [3]. Statistically, Hispanic children experience a higher age-adjusted incidence rate for acute lymphoblastic leukemia than all other demographic groups [3]. Based on these alarming statistics, we wanted to focus primarily on an acute lymphoblastic lymphoma (CEM) to identify novel anti-lymphoma cancer drugs in this study. In addition, we compared the effects of the compounds on the CEM cell line that was highly sensitive to the treatments to COLO

✉ Renato J Aguilera
raguilera@utep.edu

[1] The Border Biomedical Research Center, Department of Biological Sciences, The University of Texas at El Paso, El Paso, Texas, USA

[2] Drug Discovery and Development Research Cluster, University of Saskatchewan, Saskatoon, Canada

[3] School of Sciences, Indiana University Kokomo, Kokomo, IN, USA

[4] Division of Surgical Oncology, Department of Surgery, Department of Microbiology, Immunology and Molecular Genetics, The Molecular Biology Institute, Jonsson Comprehensive Cancer Center, AIDS Institute, The University of California, Los Angeles (UCLA), California, USA

205, which is a colon cancer cell line that was the most resistant. Colorectal cancer is the third most common cancer diagnosed in both men and women and the second most common cause of cancer-related death in both sexes combined in the United States [1]. In 2022, it was projected that 106,180 new cases of colorectal cancer would arise, causing 52,580 deaths by the end of 2022 [2]. Deaths from colorectal cancer amongst people younger than 55 years of age have increased by 2% per year from 2007 to 2016 [1]. Seeing as every case of cancer diagnosed is treated as unique, here we strive to discover a compound that has the potential to be cytotoxic amongst various cancer cell lines from different tissue origins.

In nature, piperidone-derived compounds have been found to possess anticancer activity [4]. In addition, piperidones are also known to possess antibacterial [5], antimalarial [6], anti-inflammatory [7], and antiproliferative activities [8]. Previously, our group reported that two compounds containing a piperidone structure could efficiently induce cell death in leukemia/lymphoma cells, acting as proteasome inhibitors, leading to activation of pro-apoptotic pathways [9, 10]. The overall design of the compounds was based on the considerations of tumors utilizing glycolysis for the production of energy and pyruvate dehydrogenase kinase 1 (PDK1) in order for glycolysis to occur. By doing so, the inhibition of this enzyme may diminish tumor development. With this in mind, dichloroacetic acid is a designated anticancer agent and is known to be an inhibitor of PDK1 [11]. Considerable effort has been made to prepare analogs containing the 1,5-diaryl-3-oxo-1,4-pentadienyl pharmacophore mounted on heterocyclic and cycloaliphatic scaffolds [12] [13]. Hence the formation of compounds containing both of these molecular features led to the decision to prepare 2608 and 2610 and related compounds [10]. The compounds were synthesized *via* the synthetic chemical route outlined in Fig. 1 [10]. Leading to the acid-catalyzed condensation between 4-piperidone and various substituted aryl aldehydes led to the intermediate 3,5-bis(benzylidene)-4-piperidones, which were acylated with dichloroacetyl chloride to give the desired products 2608 and 2610.

In this study, compounds 2608 and 2610 were found to exhibit broad cytotoxic activity on various cell lines. We tested both piperidones to determine the likely cause of cytotoxicity and to elucidate whether they induce reactive oxygen species (ROS) accumulation, depolarize the mitochondria, activate caspase3/7, and cause cell-cycle arrest. Our results also clearly demonstrated that the mode of action of the compounds was *via* induction of apoptosis.

Materials and methods

General procedure for synthesis of 2608 and 2610

In a 50 mL Erlenmeyer flask, 3,4-difluoro- or 3,4-dichlorobenzaldehyde (15.6 mmols) was dissolved in 10 mL of ethanol by warming the solution in a hot water bath. To this solution 4-piperidone monohydrate hydrochloride (6.50 mmols) followed by 10 mL glacial acetic acid were added at room temperature. The mixture was then bubbled with HCl gas for about 5 min. and stirred at room temperature for 24 h. The resultant precipitate was collected by vacuum filtration and resuspended in 10% aqueous K_2CO_3 solution (20 mL). The mixture was vigorously stirred overnight. The precipitate was collected by vacuum filtration and washed with water and finally dried in the oven at 50 ºC to give 3,5-dibenzylidenepiperidin-4-ones with 70–80% yield.

To a solution of an appropriate (3E,5E)-3,5-dibenzylidenepiperidin-4-one (4.8 mmol) in 1,2-dichloroethane (70 mL) was added dichloroacetyl chloride (9.6 mmol) dropwise by keeping the reaction mixture in an ice-water bath. After that triethyl amine (2.2 mmol) was added dropwise to the reaction mixture and the mixture was stirred at room temperature for 20 h. The precipitate formed was removed by vacuum filtration and the filtrate was transferred into a separatory funnel and extracted two times with 0.5 M

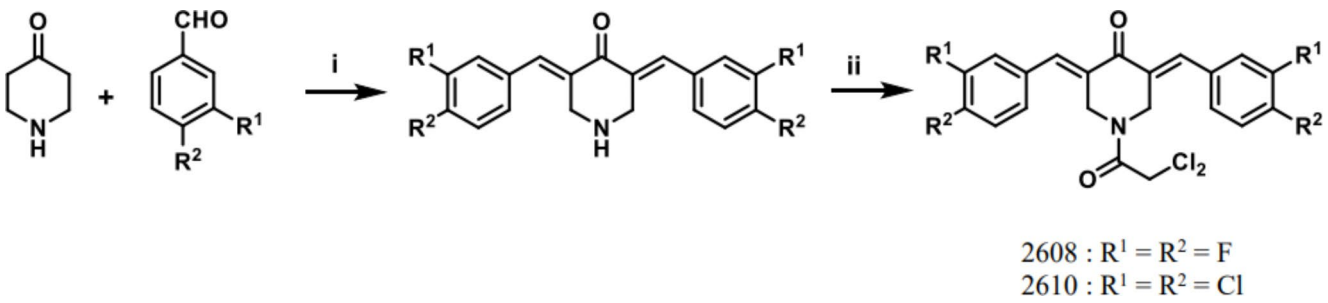

Fig. 1 Synthesis of 2608 and 2610. i = HCl/CH_3COOH, ii = $Cl_2CHCOCl$. The 2608 (1-dichloroacetyl – 3,5-bis(3,4-difluorobenzylidene)-4-piperidone) and 2610 (1-dichloroacetyl-3,5-bis(3,4-dichlorobenzylidene)-4-piperidone) structures are depicted

aqueous HCl solution (30 mL each) and one time with 30 mL water. The organic phase was dried over anhydrous sodium sulfate, filtered and evaporated using a rotary evaporator to give crude product. The crude product was dissolved in a minimum amount of dichloromethane (CH_2Cl_2) by heating the mixture in a hot water bath and then hot ethanol (about half of CH_2Cl_2 volume) was added to it. The mixture was kept overnight at room temperature for crystallization. The crystalized product was collected by vacuum filtration and washed with cold ethanol and finally dried in the oven at 50 ºC to give (3E,5E)-3,5-dibenzylidene-1-(2,2-dichloroacetyl)piperidin-4-one (2608 or 2610).

NMR of compounds 2608 and 2610

The following 1 H and 13 C NMR spectra were determined using a Bruker Avance III 500 MHz NMR spectrometer while mass spectra were generated using a QSTAR XL Hybrid LC/MS/MS system:

Compound 2608: Yield: 60%. mp 152.4-153.4 ºC; 1 H NMR ($CDCl_3$): d 7.82 (s, 1 H, =CH), 7.77 (s, 1 H, =CH), 7.25–7.15 (m, 6 H, Ar-H), 6.06 (s, 1 H, –$CHCl_2$), 5.02 (s, 2 H, NCH_2), 4.87 (s, 2 H, NCH_2). 13 C NMR ($CDCl_3$): δ 184.82, 162.24, 152.22, 152.11, 150.19, 150.09, 137.07, 136.58, 131.30, 130.89, 127.12, 126.83, 119.31, 119.16, 118.91, 118.09, 65.42, 46.90, 44.57. HRMS (FD+): m/z 457.02666 (M+), calcd 457.02595 for $C_{21}H_{13}C_{l2}F_4NO_2$.

Compound 2610: Yield: 72%. mp 161.6-162.1 ºC; 1 H NMR ($CDCl_3$): d 7.80 (s, 1 H, =CH), 7.76 (s, 1 H, =CH), 7.52–7.49 (m, 4 H, Ar-H), 7.28 (d, 1 H, Ar-H, J = 7.5 Hz), 7.22 (d, 1 H, Ar-H, J = 7.5 Hz), 6.06 (s, 1 H, –$CHCl_2$), 5.03 (s, 2 H, NCH_2), 4.86 (s, 2 H, NCH_2). 13 C NMR ($CDCl_3$): δ 184.63, 162.22, 136.78, 136.28, 134.33, 134.10, 133.47, 132.60, 131.91, 131.77, 131.52, 131.33, 131.02, 129.31, 129.07, 65.42, 46.98, 44.55. HRMS (FD+): m/z 520.90795 (M+), calcd 520.90774 for $C_{21}H_{13}C_{l6}NO_2$.

Experimental piperidones

Stock solutions of both 2608 (1-dichloroacetyl – 3,5-bis(3,4-difluorobenzylidene)-4-piperidone) and 2610 (1-dichloroacetyl-3,5-bis(3,4-dichlorobenzylidene)-4-piperidone) piperidones were initially prepared in dimethyl sulfoxide (DMSO; Sigma-Aldrich, St Louis, MO, USA), and then, further working dilutions were also made using DMSO as a solvent. As necessary, aliquots of the piperidones were added directly to 24- or 96-well experimental plates containing cells cultured in a complete growth medium. DMSO, the piperidone diluent, was consistently tested at the same concentration as contained in the experimental samples as a control for non-specific solvent effects.

Cell tissue culture

Cell tissue cultures were obtained through the American Type Culture Collection (ATCC, Manassas, VA, USA). For the culture of lymphoma and leukemia, T lymphoblast CEM (ATCC ®CRL-2265™), B lymphocyte RAMOS (ATCC ®CRL-1596™), and promyelocytic leukemia HL-60 (ATCC ®CCL-240™), multiple myeloma MM.1R (ATCC ®CRL-2975™), MM.1 S (ATCC ®CRL-2974™), U266 (ATCC ®TIB-196™), and RPMI-8226 (ATCC ®CRM-CCL-155™), along with colon cancer (COLO 205, ATCC ®CCL-222™), the RPMI-1640 medium (Hyclone, Logan UT, USA), supplemented 10% fetal bovine serum (FBS, Hyclone), 100 U/mL of penicillin and 100 µg/mL of streptomycin (Thermo Fisher Scientific Inc. Rockford, IL) was utilized. The HL-60 cells were grown using the above medium but with 20% FBS instead of 10%. The Hs-27 (ATCC ®CRL-1634™), MDA-MB-231 (ATCC ®CRM-HTB-26™), and PANC-1 (ATCC ®CRL-1469™) cell lines were grown in Dulbecco's Modified Eagle's Medium (DMEM; CORNING, Corning, NY, USA) with the addition of 10% FBS and 100 U/mL of penicillin and 100 µg/mL of streptomycin. A colorectal adenocarcinoma, HT-29 (ATCC ®HTB-38™), was cultured in McCoy's 5 A Medium supplemented with 10% FBS and 100 Units/mL Penicillin and 100 µg/mL Streptomycin. For colon fibroblast CCD-112-CoN (ATCC ®CRL-1541™), Eagles Minimum Essential Medium supplemented with 10% FBS, 100 Units/mL Penicillin and 100 µg/mL Streptomycin was used. Furthermore, MCF10A cells were grown in DMEM F12 supplemented with 10% FBS, 100 Units/mL Penicillin and 100 µg/mL Streptomycin [14]. Lastly, pancreatic carcinoma (PC-3, ATCC ®CRL-1435™) utilized F-12 K Medium supplemented with 10% FBS, 100 Units/mL Penicillin and 100 µg/mL Streptomycin. Consistently, all cell types were incubated at 37ºC in a humidified atmosphere of 5% CO_2 using a conventional water-jacketed incubator.

Differential nuclear staining (DNS) bioimaging assay to determine CC_{50}

The potential cytotoxicity of the compounds was evaluated on CEM and COLO 205 cell lines and various other cell lines using a live-cell DNS bioimaging assay[15]. Cells were grown and seeded in 96-well plates with a density of 10,000 cells per well in 100 µl of tissue culture medium. Cells were then treated with a concentration gradient (0.1 µM-5 µM) of the two piperidones for a 48 h time point. Both compounds were analyzed in each plate, including a compound solvent control (dimethyl sulfide; 1% DMSO; Millipore Sigma, St. Louis, MO USA), a positive control 1 mM hydrogen peroxide (H_20_2; Millipore Sigma, St. Louis,

MO USA), and untreated cells to monitor the background of the dead cell population. To distinguish between the live/dead cell populations, a mixture of propidium iodide (PI; Biotium; Fremont, CA, USA) and Hoechst 33,342 (Invitrogen; Eugene, OR, USA), both DNA intercalating fluorescent dyes, was added to each well (5 µg/ml each) 2 h prior to reading and incubated at 37ºC. Hoechst is a fluorescent dye that is permeable to both live and dead cells. In contrast, PI is selective and can only permeate cells whose plasma membrane has been compromised and is used primarily to label the dead cells. Images were captured from each treated well using a multi-well plate reader IN Cell 2000 analyzer (GE Healthcare; Pittsburg, PA, USA). Cytotoxic concentrations of 50% were then obtained using a linear interpolator calculator (https://www.johndcook.com/interpolator.html).

poptosis/necrosis assay

An early indication of apoptotic death is the externalization of phosphatidylserine (PS) on the cellular surface [16, 17]. With the use of flow cytometry, PS can easily be detected *via* Annexin V-FITC. CEM cells were seeded in a 24-well plate at 100,000 cell density in 1 mL of media [17]. COLO 205 cells were seeded in the same manner, respectively. The cells were then incubated overnight and treated for 24 h with 2608 and 2610 CC_{50}'s. For vehicle control, cells were treated with DMSO; as a positive control of cytotoxicity, cells were treated with 1 mM H_2O_2, and untreated control cells were used to monitor the background of the dead cell population. Cells growing in suspension were then harvested and placed in pre-chilled flow cytometric tubes. Whereas adherent cells were treated with 400 µl trypsin, incubated for 5 min, and collected in flow cytometric tubes. Cells from each well were washed with ice-cold PBS and centrifuged at 1200xRPM for 5 min. Cell pellets were then gently resuspended with annexin V-FITC and PI in 100 µl of binding buffer and incubated in the dark for 15 min on ice. Prior to analyses by flow cytometry, cells were added with 400 µl of ice-cold binding buffer. Approximately 10,000 events/cells were acquired per individual sample by using Kaluza software (Beckman Coulter). The total apoptotic cell populations are depicted as the sum of both early and late facets of apoptosis. Three independent measurements were performed, and the average and standard deviation were calculated, obtaining the percentage of both apoptotic and necrotic cells.

Analysis of mitochondrial membrane potential using JC-1 and flow cytometry

CEM and COLO 205 cells were seeded in 24-well plates and treated with 2608 and 2610 CC_{50} for an 8 h incubation. Following treatment, the cells were harvested and labeled with fluorophore 5,5,6,6-tetraethylbenzimidazolylcarbocyanine iodide (JC-1). A flow cytometer was used to capture red and green signals emitted by the cells. Healthy cells with polarized mitochondria will emit a red fluorescence signal due to the JC-1 aggregated formation [14, 16]. In contrast, once the mitochondria are depolarized, they will form JC-1 monomers exhibiting a green fluorescence signal. The controls used in this series of experiments were similar to those in the previous assay. Each data point represents the average of at least three independent measurements.

Cell cycle profile analysis *via* flow cytometry

To investigate the mechanism at which the compound induces cell arrest, CEM and COLO 205 cells were seeded in 24-well plates at a density of 100,000 cells per well in 1 ml of media [18]. CEM cells were treated with 2608 CC_{20} (0.0397 µM) and 2610 CC_{20} (0.0372 µM), and incubated for 72 h. COLO 205 cells were treated with 2608 CC_{20} (0.7616 µM) and 2610 CC_{20} (1.5164 µM) and incubated for 72 h. The controls used for these experiments were the same as described above. Following incubation, cells were collected in flow cytometric tubes, centrifuged at 1200 RPM for 5 min, and resuspended in 100 µl of room temperature media. Lastly, a single nuclear isolation medium (NIM)-DAPI reagent was added to each flow cytometry tube (200 µl) and analyzed *via* flow cytometry [14, 19]. This dye is able to stain the cell nuclei facilitating the quantification of the total amount of DNA per cell. Roughly 10,000 events/cells were acquired per sample (Gallios; Kaluza software; Beckman Coulter). For this purpose, the FL-9 detector and 405 nm laser were solely responsible for quantifying the total DNA content for each event (cell) and distributing them to the designated subpopulation. Each experimental point and its corresponding controls were performed using at least three independent measurements.

Caspase-3/7 activation

The cellular activation of caspase 3/7 was detected by adding the cell membrane-permeable fluorogenic NucView 488 caspase 3/7 substrate [20]. This substrate can permeate living cells with an intact plasma membrane and allow for identifying active caspase 3/7. The cells were examined *via* flow cytometry with the same plating methodology, as previously mentioned [17] and treated with their 24 h CC_{50} respectively (CEM 2608 CC_{50} 0.0993 µM and 2610 CC_{50} 0.0932 µM and COLO 205 2608 CC_{50} 1.904 µM and 2610 CC_{50} 3.791 µM). Cells were harvested in flow cytometry tubes and centrifuged at 1200 RPM for 5 min. Cell pellets were gently resuspended in 200 µl of PBS, containing 5 µl

of NucView488 caspase 3/7 substrate, and incubated in the dark for 45 min at room temperature. After this step, 300 µl of PBS was added to each flow cytometry tube. A green fluorescent signal indicated caspase 3/7 activation within the cell during the analysis. Furthermore, 10,000 events were assessed per sample. Each sample was performed at least three times. For sample acquisition and analysis purposes, the Kaluza software was utilized (Beckman Coulter).

Reactive oxygen species

The production of ROS signals for oxidative damage in the mitochondria by retrograde redox signaling was investigated [21]. Analysis of ROS production in CEM and COLO 205 cells treated with twice the CC_{50} concentration of 2608 and 2610 24 h was conducted via carboxy-H2 DCFDA (6-carboxy-2' 7'dichlorodihydrofluorescein diacetate) fluorescein reagent (Invitrogen, C400) and analyzed by flow cytometry. CEM and COLO 205 cells were seeded in a 24-well plate at a density of 100,000 cells per well in 1mL of culture medium. CEM and COLO 205 cells were treated with compounds 2608 and 2610 8 h prior to reading. The controls mentioned above were used for this experiment, as well. Cells were collected and placed in flow cytometry tubes and centrifuged for 5 min at 1200 RPM. Cells were gently resuspended in PBS containing carboxy-H2 DCFDA (master mix/loading buffer) and incubated for 1 h. Cells were then centrifuged again to remove the excess loading buffer and resuspended in 500 µl of fresh PBS. Immediately after, cells were analyzed *via* flow cytometry, acquiring ~ 10,000 events (cells) per sample. Cytometry analysis was performed as in the previous section.

Analysis of poly-ubiquitinated proteins in CEM and COLO 205

A total of 3,000,000 CEM and COLO 205 cells were seeded in T-25 flasks in 10 ml of complete RPMI medium. Cells were then treated with 10 µl of the 2x CC_{50} of CEM (0.198 µm) and COLO 205 (3.808 µm) 2608, 2610 (CEM; 0.186 µm, COLO 205; 7.582 µm), MG-132, and the vehicle PEG-400 (0.3%) at an 8-hour time period. Following incubation, the cells were then harvested in 15 ml conical tubes to form pellets and transferred to 1.5 ml tubes. The cells were then washed once with 1 ml PBS and pelleted at 1000 g for 6 min. Once pelleted, the PBS was removed, and the pellet was resuspended in 70 µl 2x Laemmli buffer (120 mM Tris-HCl, 0.1% β-mercaptoethanol, 4% SDS, 20% glycerol, and 0.02% bromophenol blue) and boiled at 100 C for 15 min to lyse the cells. Protein was then quantified utilizing a Nano-Drop N-1000 system, and a total of 100 µg per sample was calculated. The final volume of 25 µl was loaded per lane on a 7% SDS PAGE gel and separated at 100 V for 1.5 h. The gel was then transferred to a PVDF membrane at 100 V for 1 h. Afterward, the PVDF membrane was blocked overnight at 4 C in 5% powdered milk. Following the overnight incubation, the primary antibody, mouse monoclonal anti-Ubiquitin (Santa Cruz Biotech; sc-8017) was added to the membrane and incubated for 1 h. The membranes were washed with TBS-T 3 times for 15 min. The secondary polyclonal goat anti-mouse antibody (1:10,000 diluted in TBS-T) conjugated to horseradish peroxidase (Thermo Fisher; 31,430) was added and incubated at room temperature for 1 h. The membrane was then rewashed with TBS-T 3 times for 15 min to wash away any unbound antibodies. Prior to the reading, the membrane was placed in the iBright machine and labeled with Enhanced Chemiluminescence Solution (ECL), one part being 1 mL peroxide and 1mL of luminol. The ECL is based on the antibodies that are conjugated to the membrane or labeled with horseradish peroxidase [22]. The addition of the luminol produces excited intermediates, and upon release, it emits a blue signal [22]. Following the wash, the membrane was then read with the Invitrogen iBright Imaging Systems and quantified for further analysis.

Computational docking

The initial docking was performed utilizing the Schrödinger software suite (Schrödinger, LLC, New York, NY, USA). The protein crystal structure was used for this docking experiment utilizing the protein data bank (https://www.rcsb.org/). The protein targets used for these experiments were UCH-L5 (PDB: 3IHR) and USP14 (2AYO) and were prepared as previously described [23]. Using the Maestro 12.8 interface and Protein Preparation Wizard, the crystalized 3-dimensional figures were prepared. The program was left to run as default, and the options for missing side chains, missing loops, the removal of water, and any other interfering ligands were the only ones selected. Prior to docking, the compounds were optimized and then minimized to expose hidden crystal structures using the Schrödinger Release 2018: LigPrep, Schrödinger, LLC, New York, NY, 2018 interface of the Schrodinger software, with Optimized Potentials for Liquid Simulations 4 force field, at a pH 7 ± 2 using Schrödinger Release 2018: Epik, Schrödinger, LLC, New York, NY, 2018 (OPLS4 force field) [24]. Specific Residues that have been previously identified to form the binding pocket of b-AP15 were used for the receptor grid generation utilizing Schrödinger Release 2021-3: Induced Fit Docking protocol; Glide, Schrödinger, LLC, New York, NY, 2021; Prime, Schrödinger, LLC, New York, NY, 2021 [24]. This generates a binding grid around amino acids Asn85, Cys88, Ala162, and Leu181 for UCH-L5, and

Asn109, Cys114, Ser433, Ser432, and Gly434 for USP14. Lastly, molecular mechanics (MM-GBSA) of the docked compounds was performed using the Prime tool on Maestro 12.8 **Schrödinger Release 2018**: Prime, Schrödinger, LLC, New York, NY, 2018, and the best scoring compounds were selected.

Statistical analyses

Every experimental point indicates a minimum of three independent measurements unless otherwise stated. The findings were displayed as the average of the several measurements with their corresponding standard deviations to denote the experimental variability. The Linear Interpolator software was utilized to obtain the 50% cytotoxic concentration (CC_{50}) (https://www.johndcook.com/interpolator.html; accessed on 24 February 2022). Here, the CC_{50} is defined as the compound's concentration required to kill 50% of the cell population. The *P*-values were calculated using a two-tailed paired Student's *t*-test to establish statistical significance between two samples, using the *T*-Test Calculator for 2 Independent Means software (https://www.socscistatistics.com/tests/studentttest/default2.aspx; accessed on 24 February 2022). On some circumstances, the significant *P*-values (≤ 0.05) were annotated with asterisks; * $P < 0.05$, ** $P < 0.01$, and *** $P < 0.001$.

Results

Determination of cell death induction *via* the live-cell Differential Nuclear Staining (DNS) cytotoxicity assay

The cytotoxic effects of 2608 and 2610 piperidones were analyzed using the DNS imaging assay on twelve human cancer cell lines and two non-cancerous fibroblast cell lines. The DNS assay is reliable and validated for primary and secondary screens for potential anticancer cytotoxic experimental compounds [14, 15] [25]. This assay utilizes Hoechst fluorescent dye that permeates both living and dead cells when treated 2 h before reading [26]. In addition, PI stains the nucleus of dead or dying cells with a compromised plasma membrane. As indicated in Table 1, both 2608 and 2610 piperidones display a range of cytotoxicity across various cancer cell lines tested. The cell lines that were grown in suspension, lymphoma, leukemia, and multiple myeloma cell lines, CEM, RAMOS, U266, RPMI-8226, MM1R, MM1S and HL-60, were incubated for 48 h with 2608 or 2610 to obtain the CC_{50} values. The adherent cell lines, HT-29, MDA-MB-231, PC-3, Hs-27, PANC-1, CCD-112-CoN, COLO 205, and MCF-10 A, were initially incubated overnight to allow their attachment to the bottom of the plate, in the absence of the experimental compounds. Next, a concentration gradient of the piperidones was added to the cells and incubated for an additional 48 h, obtaining a dose-response curve to calculate the concentration at which 50% (CC_{50}) of the cell population dies. The CC_{50} values ranged from 0.02 µM on CEM to 1.1 µM on PANC-1 cell lines.

Table 1 2608 and 2610 cytotoxic concentrations 50% (CC_{50}) on various cancer cell lines at a 48 h time point

		2608			2610		
CELL TYPE	**CELL LINE**	**CC_{50}(µM)**	**S.D.**	**SCI**	**CC_{50}(µM)**	**S.D.**	**SCI***
Acute Lymphoblastic Lymphoma	CEM	0.02	0.003	22.75	0.03	0.004	6.66
Burkitt's Lymphoma	RAMOS	0.095	0.041	4.789	0.036	0.005	5.55
Acute Promyelocytic Leukemia	HL-60	0.064	0.041	7.109	0.024	0.011	8.33
Breast Adenocarcinoma	MDA-MB-231	0.047	0.008	9.68	0.121	0.055	1.65
Breast Epithelial	MCF-10 A	0.175	0.007	2.6	0.120	0.004	1.66
Colorectal Adenocarcinoma	HT-29	0.162	0.021	2.80	0.036	0.004	5.55
Colorectal Adenocarcinoma	COLO 205	0.424	0.010	1.07	1.664	0.184	0.12
Colon Fibroblast	CCD-112-CoN	0.12	0.042	-	0.176	0.015	-
Normal Foreskin Epithelial	HS-27	0.455	0.035	-	0.2	0.028	-
Pancreatic Carcinoma	PANC-1	1.132	0.259	0.40	0.4135	0.045	0.48
Prostatic Adenocarcinoma	PC-3	0.301	0.005	1.51	0.446	0.003	0.44
Multiple Myeloma	U266	0.0144	0.001	31.59	0.762	0.010	0.26
Multiple Myeloma	RPMI-8226	0.0397	0.002	11.46	0.3335	0.031	0.599
Multiple Myeloma	MM1 S	0.0181	0.0007	25.138	0.0261	0.0028	7.66
Multiple Myeloma	MM1 R	0.0160	0.001	28.43	0.009	0.005	22.22

***SCI: Selective cytotoxicity index values were calculated using the following equation: $CC_{50}$of non-cancer cells divided by the $CC_{50}$of the cancer cell line. SCI calculated using Hs-27 as non-cancer cell line**

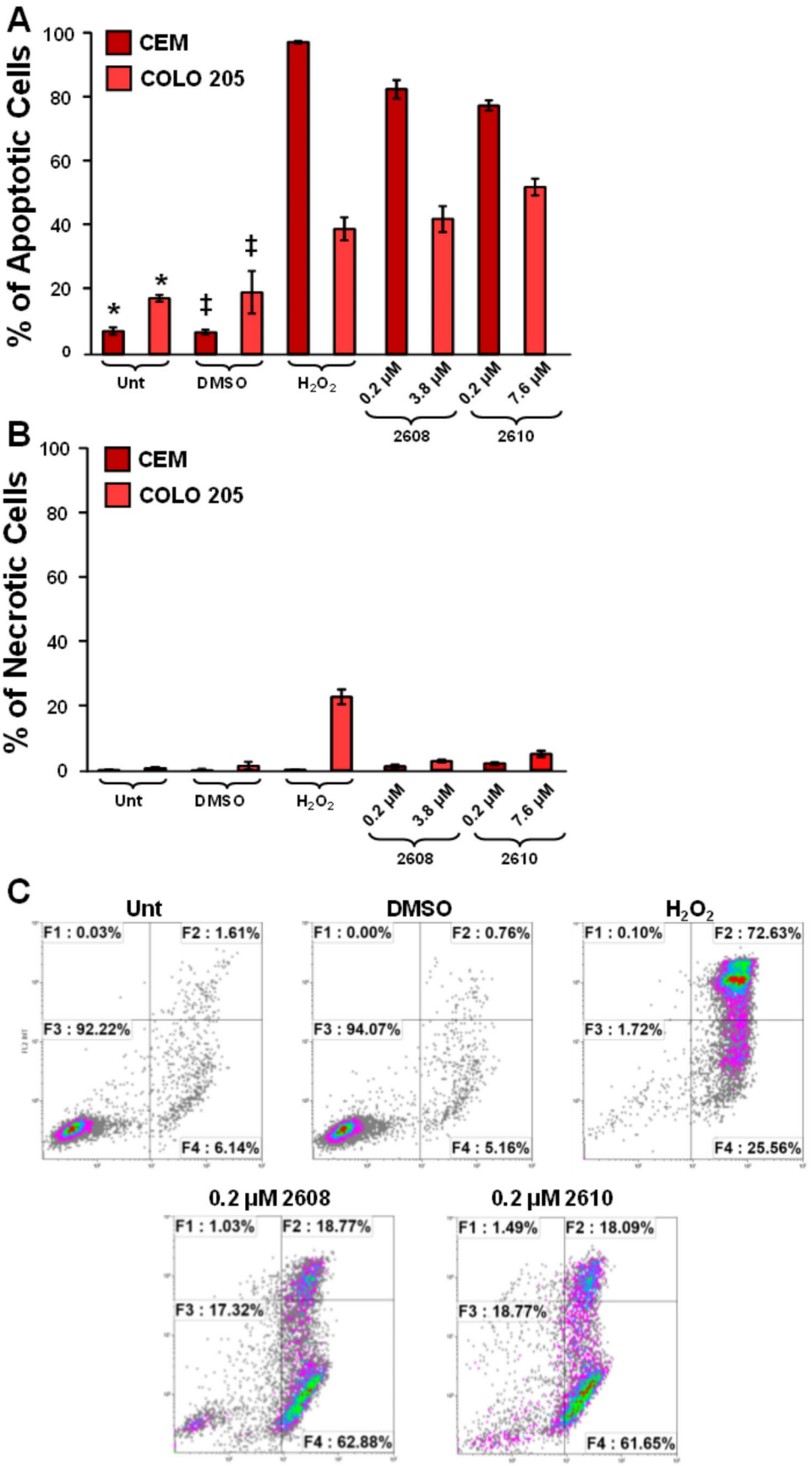

Fig. 2 Both experimental piperidones induce significant PS externalization in CEM and COLO 205 cells in a dose-dependent modality. Cells were exposed to the experimental piperidones for 24 h, and cells were then stained with Annexin V and PI and monitored via flow cytometry. The concentrations of the compounds are shown for each treatment and represent twice the CC_{50} values for each cell line (see Table 1). Figure 2 A and 2B contain the percentage of apoptotic cells that are Annexin V-FITC positive, whereas panel 2b shows the percentage of necrotic cells that are PI-positive Annexin V-FITC negative. The following controls were included: DMSO as solvent control, 1 mM H_2O_2 was incorporated as a positive control for cytotoxicity, and untreated (Unt) cells. Statistical analyses were accomplished using a two-tailed Student's paired t-test. The asterisk (*) annotations compare untreated cells with 2X CC_{50} of both 2608- and 2610-treated cells with P-values of < 0.00001 and 0.00001 for CEM and P-values of < 0.007 and 0.0001 for COLO 205, respectively. The double dagger symbols (‡) compare the DMSO-treated cells with CC_{50} of 2608- and 2610-treated cells with P-values of < 0.00001 and 0.00001 for CEM and P-values of < 0.0005 and 0.00003 for COLO 205, respectively. Representative flow cytometric dot plots were used in panel C to create the bar graphs corresponding to CEM cells

Analyses of phosphatidylserine (PS) externalization using the Annexin V/PI assay

To determine whether both 2608 and 2610 cause cell death *via* apoptosis or necrosis, we measured the externalization of phosphatidylserine (PS) in CEM and COLO 205 cells, respectively, using an annexin-V-FITC/PI assay. For this assay, we used the 2x CC_{50} concentrations determined on COLO 205 for both 2608 and 2610 CEM (see Fig. 2 for details). The data indicate significant PS externalization compared to the DMSO solvent control for both cell lines. As expected, a high percentage of PS externalization was detected when cells were treated with the positive control H_20_2 (39%), whereas DMSO and untreated cells showed low PS externalization (18–19%). Furthermore, the results indicate that both compounds triggered apoptosis to induce cell death due to the significant percentage of PS externalization in CEM and COLO 205. However, PS externalization was more pronounced in the CEM cell line.

Piperidone compounds induce an accumulation of reactive oxygen species (ROS)

To further examine the mechanism by which 2608 and 2610 induce cell death, the accumulation of ROS in CEM and COLO 205 cells was measured after treatment of cells with the piperidones for 6 h with the 24 h CC_{50} concentration. We incubated for 6 h in order to detect ROS generation since a longer incubation time would not have been advantageous; as ROS generation occurs in the early stages of apoptosis [27]. Following the exposure to the 24 h CC_{50} for both compounds, the cells were incubated for one hour with 10 µM

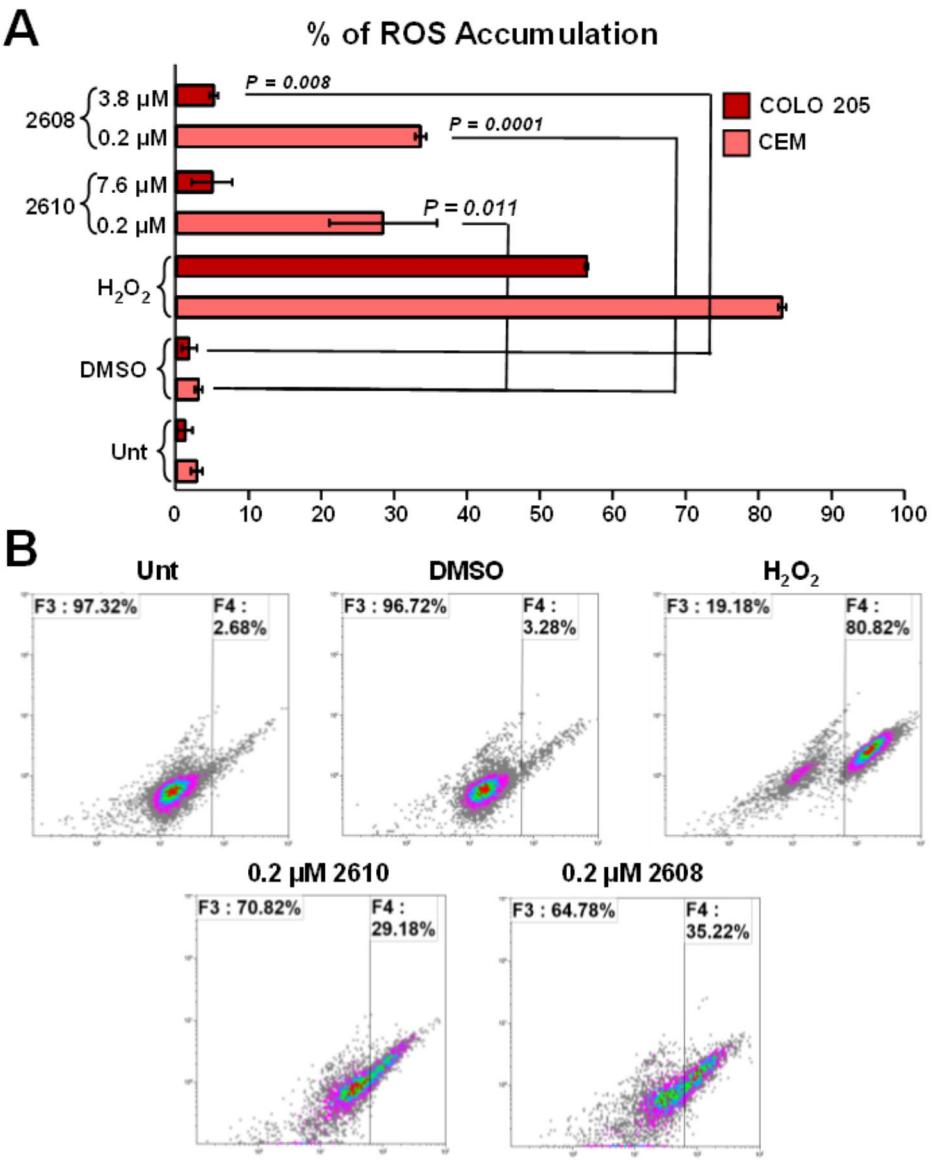

Fig. 3 Significant ROS induced by 2610 and 2608 piperidones on CEM and COLO 205 cells as compared with the DMSO-treated cells. Statistical analyses were acquired by using the two-tailed Student's paired t-test. H_2O_2 (1 mM)-treated cells were included as an oxidative stress positive control. Representative flow cytometric dot plots were used in panel B to create the bar graphs corresponding to CEM cells

of carboxy-H2 DCFDA ROS. Subsequently, the cells were analyzed *via* flow cytometry for those emitting a green signal indicating ROS accumulation. As shown in Fig. 3, both CEM and COLO 205 cells generated ROS in the presence of the 2x CC_{50} of 2608 and 2610, indicating the induction of the intrinsic apoptotic pathway. However, the accumulation of ROS was more prominent in the CEM cell line than in COLO 205.

Induction of mitochondrial depolarization by piperidones 2608 and 2610

High ROS production levels are known to lead to mitochondrial depolarization, including damage of DNA, proteins, and lipids [28] [29]. To further investigate the mechanism by which 2608 and 2610 induce cell death, we evaluated both compounds in CEM and COLO 205 cells using the JC-1 polychromatic fluorescent reagent and flow cytometry. Both CEM and COLO 205 cells were incubated for 6 h with the compounds, and the mitochondrial membrane potential was examined. This analysis revealed that the piperidones induced significant mitochondrial depolarization at their CC_{50} and twice the CC_{50} concentrations compared to the untreated and DMSO-treated cells for CEM and COLO 205 (Fig. 4). Overall, these findings further confirm that compounds 2608 and 2610 are able to depolarize the mitochondria, indicating that the compounds induce apoptotic death.

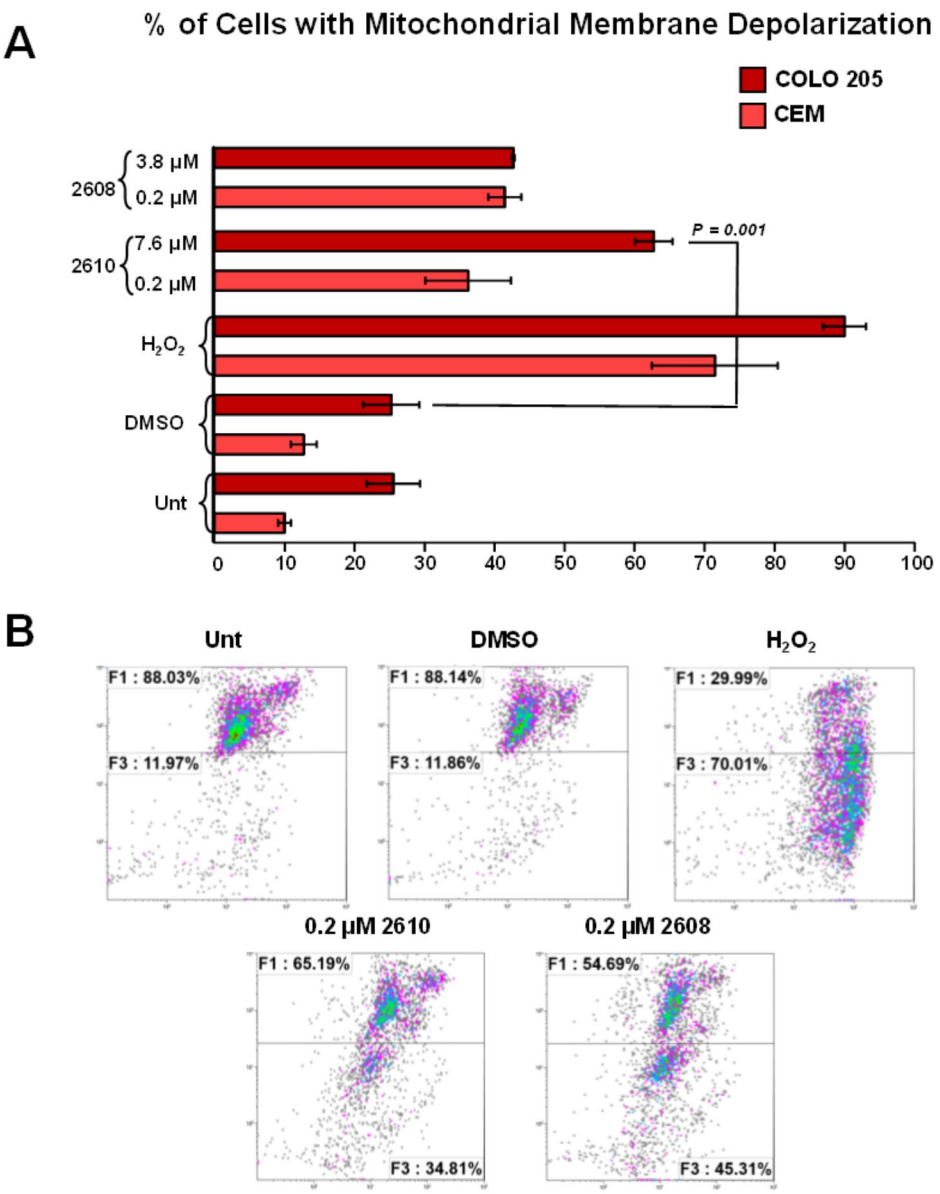

Fig. 4 The experimental piperidones induced significant mitochondrial depolarization activity on COLO 205 and CEM cells. Cells were incubated for 6 h with the experimental piperidones and then stained with JC-1 reagent and monitored by flow cytometry. Statistical analyses were acquired by using the two-tailed Student's paired t-test. The asterisk annotations on each bar graph represent the statistical significance of the experimental treatments compared with the vehicle control (1% DMSO). Cells treated with 1 mM H_2O_2 were included as an inducer for mitochondrial depolarization. Representative flow cytometric dot plots were used in panel B to create the bar graphs corresponding to CEM cells

Treatment of cancer cells with the novel piperidones leads to activation of caspases

It is known that the activation of caspase-3/7 is a biological marker of a cell undergoing apoptosis [30]. Individual caspases mediate apoptosis and various other biological processes [30]. In this study, we analyzed the activation of caspase-3/7 *via* flow cytometry by using a live-cell NucView 488 caspase-3/7 fluorogenic enzyme substrate after 7.5 h of incubation of CEM and COLO 205 cells with both piperidones. As shown in Fig. 5, a significant amount of caspase-3/7 activation was detected at the CC_{50} and twice the CC_{50} concentrations of both compounds compared to the untreated and vehicle control cells. For the positive control, H_2O_2-treated cells were significant for caspase-3/7 activation (Fig. 5). These results showed that compounds 2608 and 2610 induce cell death through the caspase-3/7 activation pathway for both cell lines, a hallmark of apoptosis.

Alteration of the cell cycle by the novel piperidones

A cell cycle analysis was conducted in order to determine if compounds 2608 and 2610 induce cell cycle alterations and ultimately cause the arrest and antiproliferative cellular activity. The cell cycle profile was examined *via* flow cytometry utilizing the DNA intercalating agent, DAPI (4',6-diamidino-2-phenylindole). Both CEM and COLO 205 cells were treated with a low concentration of 2608 or 2610 (CC_{20} concentrations) and incubated for 72 h. It

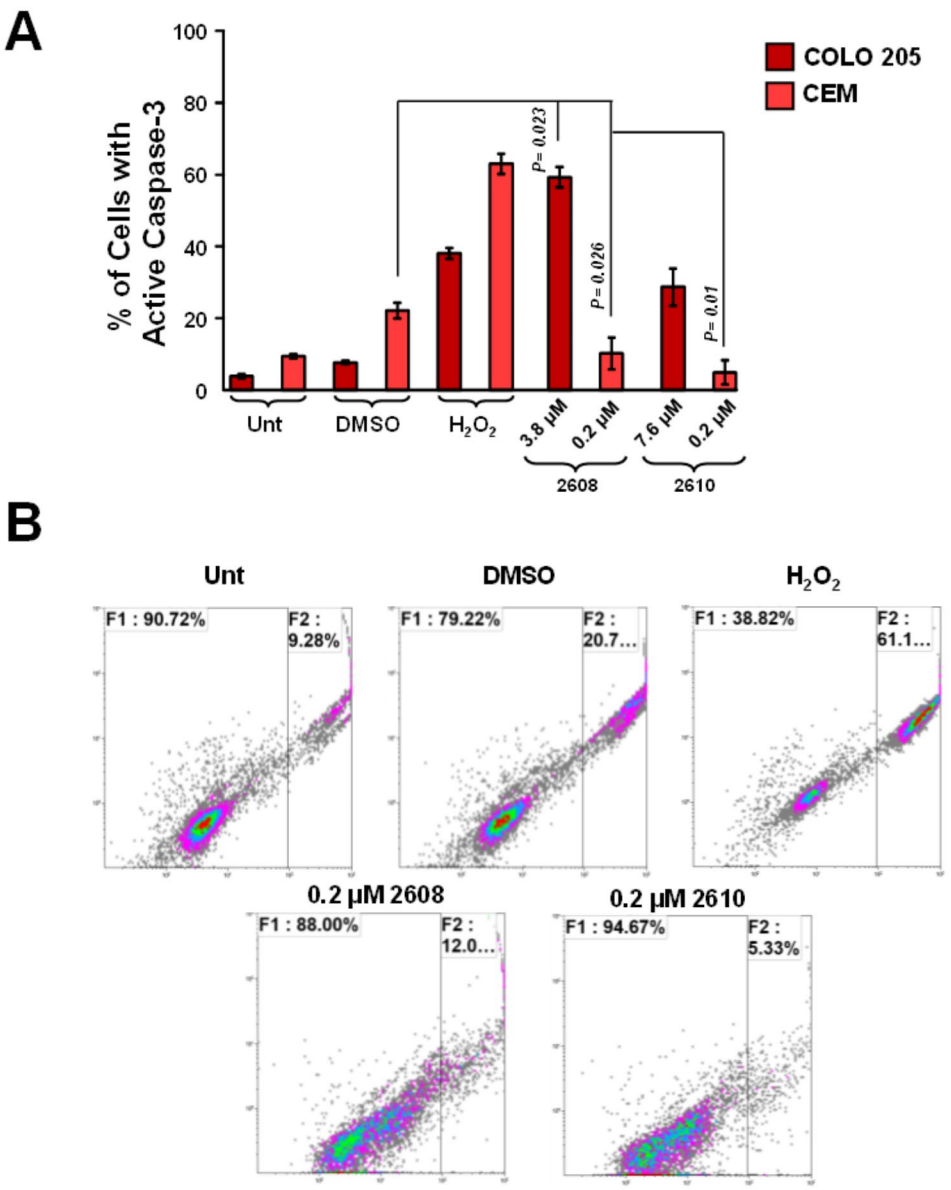

Fig. 5 Both 2610 and 2608 piperidones induce significant caspase-3/7 activation in COLO 205 and CEM cells. Cells were incubated for 7.5 h with the piperidones, stained with NucView 488 caspase 3/7 substrate, and analyzed via flow cytometry. Statistical analyses were obtained by using the two-tailed Student's paired t-test. The statistical significance of the experimental treatments compared with the vehicle control (1% DMSO). Cells treated with 1 mM H_2O_2 were included as a caspase-3/7 activator control. Representative flow cytometric dot plots were used in panel B to create the bar graphs corresponding to CEM cells

is important to note that at the CC_{50} concentrations of both compounds, extensive DNA degradation was observed in both cell lines that interfered with the cell cycle analyses (data not shown). Low concentrations of compound (CC_{20}) were used to monitor the cell cycle cycle. As in those presented in the other sections, the same controls were used in this experimental series. After incubation, both 2608 and 2610 did not alter the cell cycle profile in the cell lines tested, CEM and COLO 205 (Fig. 6). Given the data, 2608 induced DNA fragmentation in CEM cells but not in COLO 205. In comparison, 2610 caused DNA fragmentation on both cell lines, CEM and COLO 205 (Fig. 6 A). The *P*-values of DMSO-treated CEM cells compared with 2608 and 2010 treated CEM cells were 0.0036 and 0.011, respectively. The *P*-value of COLO 205 DMSO treated cells compared with 2608 treated COLO 205 cells was insignificant, whereas when compared with 2610 treated COLO 205 cells was 0.0038. Thus, the DNA fragmentation activity of 2608 was selective on CEM cells, whereas 2610 exhibited this activity on both cell lines tested. Also, both 2608 and 2610 compounds did not induce arrest in any cell cycle facets.

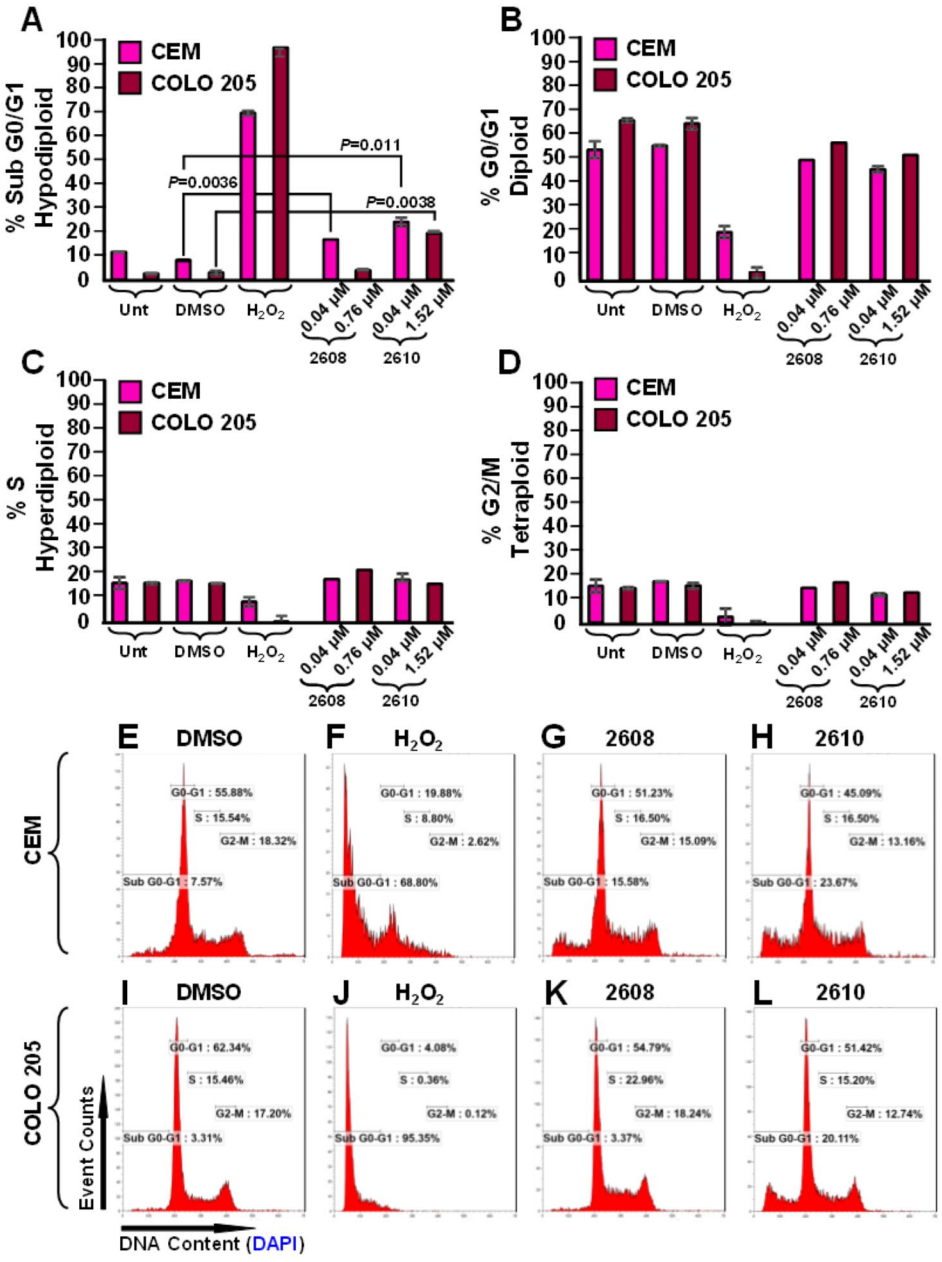

Fig. 6 2608 elicited selective DNA fragmentation on just CEM cells, and 2610 induced significant DNA fragmentation on CEM and COLO 205 cells (**A**; sub G0/G1), without arresting them in a particular cell cycle phase (**B**, **C**, and **D**). The P-values of DMSO-treated CEM cells compared with 2608 and 2010-treated CEM cells were 0.0036 and 0.011, respectively. The P-value of DMSO-treated COLO 205 cells compared to 2610 treated COLO 205 cells was 0.0038. Each bar denotes an average of three independent measurements, and the error bars correspond to standard deviation. In panels E-L, representative flow cytometric dot plots used to create the bar graphs, corresponding to CEM and COLO 205 cells

Analysis of poly-ubiquitinated proteins in CEM and COLO 205 cells

In prior reports, several piperidones have been found to disrupt proteasome activity leading to the induction of proteotoxic stress and apoptosis [31]. Proteosome inhibitors have been investigated due to their selective toxicity on cancer cells[32]. The disruption has been previously shown to result in an accumulation of polyubiquitinated proteins and inhibition of proteasomal activity [31]. The accumulation of polyubiquitinated proteins with compounds 2608 and 2610 were evaluated by western blotting after an 8 h treatment. Following densitometric quantification of high molecular weight poly-ubiquitinated proteins, the results denoted a strong increase in polyubiquitinated protein accumulation for compound 2610 in COLO 205 (1.41-fold increase), closely similar to the increase seen in the MG132 proteasome inhibitor control (1-fold increase). However, only a slight 0.61-fold increase was observed in CEM cells for this compound. Compound 2608 also showed a moderate increase in the accumulation of polyubiquitinated proteins in COLO 205 and CEM; 0.40- and 0.59-fold increase, respectively (Fig. 7).

Computational docking of UCHL5

In previously published work, a structure relationship study was performed on piperidone b-AP15 (VLX1500) revealed that this compound acted as a proteasome inhibitor, specifically interacting with Deubiquitinases (DUBs) Ubiquitin-Specific Protease 14 (USP14) and Ubiquitin C-terminal Hydrolase L5 (UCHL5) [24]. USP14 and UCHL5 and two cysteine proteases constitute the deubiquitinating enzymes within the 19 S regulatory particle in proteasome 26 S [33–36]. The 26 S proteasome contains one or two 19 S regulatory particles necessary for substrate recognition, deubiquitination, unfolding, and translocation [37, 38]. Based on the similar chemical structure of our compounds

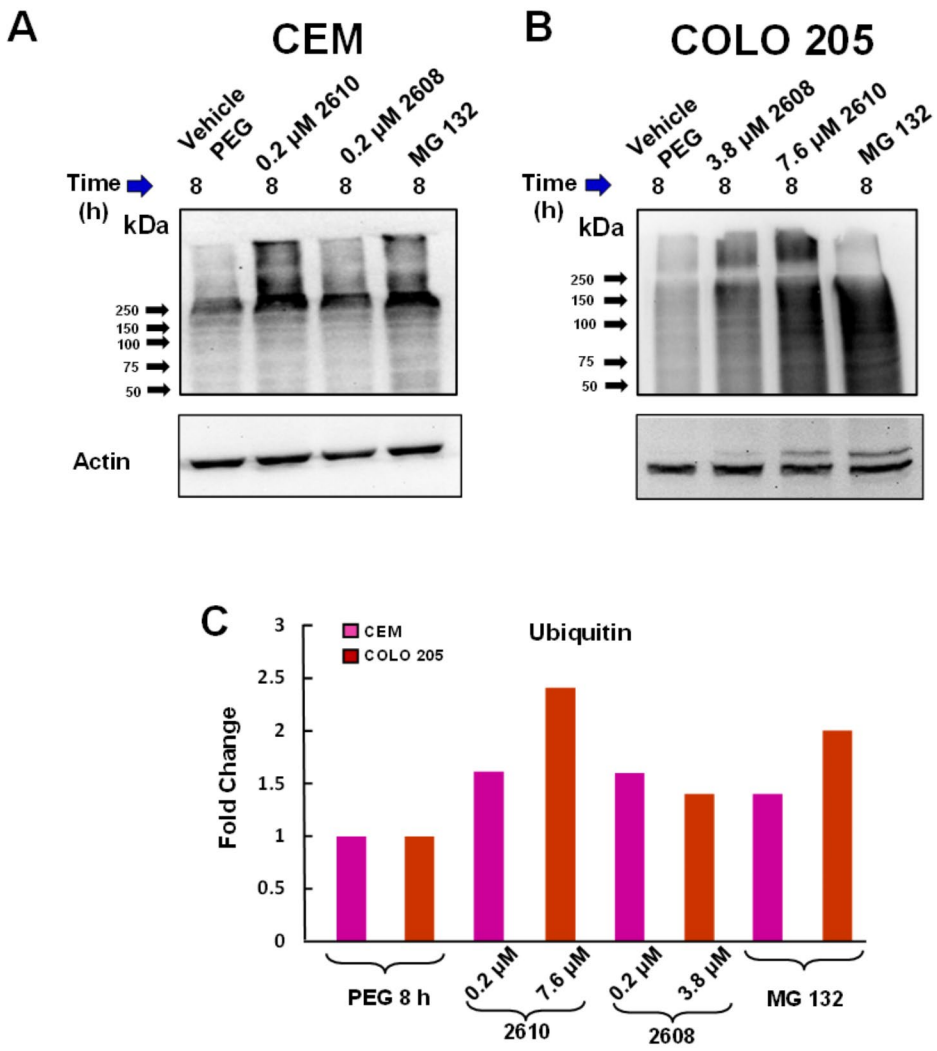

Fig. 7 Western Blot analysis reveals an accumulation of high molecular-weight poly-ubiquitinated proteins for both COLO 205 and CEM cell lines. Cells were treated for 8 h time point with; PEG 400 (vehicle control), MG 132 (positive control for proteasomal inhibition), and compounds 2610 and 2608 at a 2X CC_{50} concentration. Panel A indicates western blot analysis performed in CEM cells treated with 2610 and 2608, whereas Panel B shows analysis in COLO 205 cells with compounds 2610 and 2608. Panel C quantifies high molecular weight poly-ubiquitinated proteins (above 50 kDa) by densitometry. Fold change values for both CEM and COLO 205 are displayed

to piperidone b-AP15, we attempted to determine if they could also interact with USP14 and UCHL5. Utilizing the b-AP15 docking site and PDB code 3IHR, which has been used to generate the grid for docking, we performed *in silico* docking to this site with compounds 2608 and 2610 [24]. The binding affinity b-AP15 to the pocket of UCH-L5 was compared to the potential binding affinities of 2608 and 2610. To expose the hidden pocket in the crystal structure of b-AP15 (PDB: 3IHR), we utilized induced-fit docking to reveal and expose the binding site [24]. The analogs previously described share an α, β- unsaturated carbonyl group that is likely to react with the Cys88 found in said hidden binding pocket [24]. Our docking results confirm the previous experiment with the α, β- unsaturated carbonyl group (Michael acceptors) in proximity with Cys88 [24]. This docking would likely result in covalent binding, making the irreversible molecules inhibitors of UCHL5. With this in mind, compounds 2608 and 2610 lacked α, β- unsaturated carbonyl group, which resulted in a different binding mode and scored higher than b-AP15. Molecular mechanics were then used to approximate the binding affinity between the protein and the ligand of b-AP15, 2608, and 2610 to UCHL5, resulting in high scores relative to b-AP15, as seen in Fig. 8. Both compounds MM/GSA scores 2608 (-68.34 kcal/mol) and 2610 (-73.27 kcal/mol) fell well within the binding score of b-AP15 (-69.25 kcal/mol), indicating that both compounds are likely inhibitors of UCHL5 and bind with relatively good affinity. These results suggest that, like b-AP15, both compounds cause proteasome inhibition.

Computational docking of USP14

USP14 plays an essential role in proteasomal degradation [39]. The USP14 has been used to inhibit proteasomal function inducing apoptotic cell death in cancers [39]. As stated above, we utilized USP14 and UCHL5 to compare the docking scores of b-AP15 to our piperidones 2608 and 2610 to observe similarities. The compounds were docked using the same methodology described above with PDB code 2AYO. The best scoring poses of b-AP15 were chosen and used for molecular dynamics (MM-GBSA), which resulted in the binding affinity of -50.76 kcal/mol [24]. The binding affinity of 2608 and 2610 was estimated to be -53.82 kcal/mol and – 56.10 kcal/mol, respectively. These results suggest that both can function similarly to b-AP15 inhibiting USP14 function and blocking access to the c-terminus of ubiquitin (25).

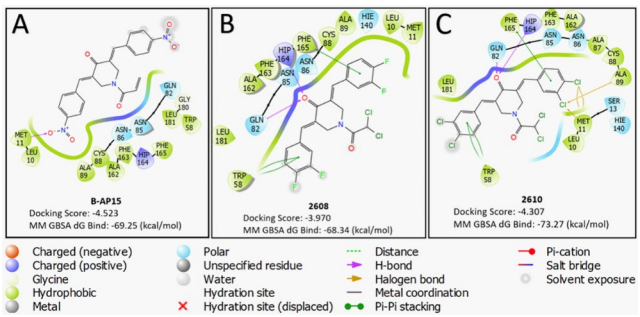

Fig. 8 Computational docking of b-AP15 (A), 2608 (B), and 2610 (C) to UCHL5. Exhibited docking scores of, 2608 (-68.34 kcal/mol) and 2610 (-73.27 kcal/mol). Both compounds fell within the score of b-AP15, -69.25 kcal/mol, indicating potential inhibition of UCHL5

Discussion

Previously, it has been shown that piperidone compounds have been highly cytotoxic toward various cancer cell lines [40]. In addition, structurally similar piperidones, P3, P4, and P5 have demonstrated cytotoxic effects towards tumorigenic cells, as opposed to non-cancerous cells, at the low micromolar range [41]. The treatment of the compounds induced apoptosis via the intrinsic apoptotic pathway and the accumulation of poly-ubiquitinated proteins and the pro-apoptotic protein Noxa [41]. This study demonstrated that both 2608 and 2610 piperidone compounds exhibited cytotoxic activity on 14 different cancer cell lines, ranging from hematological cancers to solid tumors, with CC_{50} values fluctuating from nanomolar to low micromolar concentrations (0.009 μM to 1.664 μM). Compounds P3, P4, and P5 demonstrated lower cytotoxicity in CEM and COLO 205 with CC_{50} values ranging from 0.65 μM -0.87 μM for CEM and 0.80 μM -4.66 μM for COLO 205 [41]. Additionally, we examined the effects of the compounds on a non-cancerous cell line and denoted SCI values (Table 1). Of the two compounds, 2608 displayed the highest selectivity (SCI above 5) in most cell lines compared to 2610. For these assays, we utilized a cell line that was most sensitive to the compounds,

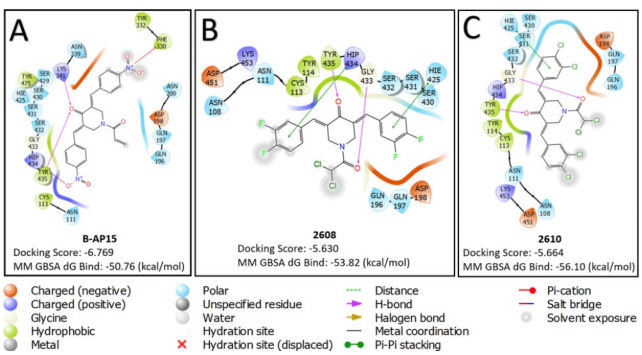

Fig. 9 Computational docking of b-AP15 (A), 2608 (B), and 2610 (C) to USP14. Exhibited docking scores of, 2608 (-53.82 kcal/mol) and 2610 (-56.10 kcal/mol). Both compounds fell within the score of b-AP15, -50.76 kcal/mol, indicating potential inhibition of UCHL5 and USP14

CEM, and one that is most resistant, COLO 205, to determine if the compounds elicited different responses that may display their resistance or sensitivity to the compounds. Once treated with a cytotoxic compound, cells can undergo apoptosis or necrosis as a cell death mechanism [42]. Thus, we investigated the cell death mechanism induced by both piperidones. Hallmarks for apoptosis include the externalization of phosphatidylserine, mitochondrial membrane depolarization, reactive oxygen species generation, and the activation of executioner caspase-3 [43]. After conducting the Annexin V/PI assay, it was determined that both 2608 and 2610 induce cell death *via* the apoptotic pathway due to the significant PS externalization in both cell lines. In cells undergoing programmed cell death, phosphatidylserine translocates to the outside of the cell membrane and is characteristic of apoptosis [16, 26].

When a cell undergoes apoptosis, it can go through the intrinsic or the extrinsic cell death pathway [44]. The intrinsic pathway implicates releasing factors by the mitochondria within the cell [45]. Caspase-3 is also activated by the permeabilization of the outer mitochondrial membrane and by releasing apoptogenic proteins that signal cell death [45]. On the other hand, the extrinsic pathway initiates apoptosis through cell membrane proteins known as death receptors [44]. A mitochondrial depolarization (JC-1) assay was conducted to investigate the depolarization of the mitochondria, which usually occurs when the cell is undergoing apoptosis *via* the intrinsic pathway. Both compounds induced significant mitochondrial depolarization for both cell lines. This depolarization was more prominent in the CEM cell line, proving that the compounds act via the intrinsic apoptotic pathway, as shown in Fig. 4.

To further investigate and characterize the mechanism by which 2608 and 2610 induce cell death, we studied ROS generation after compound treatment of CEM and COLO 205 cells. The generation of ROS plays a role in the intrinsic apoptotic cascade by being released after the mitochondria's membrane is depolarized [27, 46] It is well known that the overproduction of ROS can cause cellular stress, activate caspases, and lead to the induction of cell death [43, 47]. As shown in Figs. 3, 2608 and 2610 induced ROS overproduction in a dose-dependent manner on CEM cells. Activation of apoptosis was significant with compound 2608 in COLO 205.

When mitochondria are used to initiate the apoptosis cascade (intrinsic pathway), frequently due to the ROS overproduction, its membrane potential is disrupted during the early stages of the program, ending in its depolarization [48]. Due to mitochondrial depolarization, a downstream effector enzyme, caspase-3, is activated [49]. Caspase-3 is the enzyme where the intrinsic and extrinsic apoptotic pathways converge [50]. Typically, apoptotic cell death is irreversible after caspase-3 is activated [51, 52]. To confirm the progression facets of apoptosis induced by the two piperidones, caspase-3/7 activation was evaluated in CEM and COLO 205 cells. As expected, these assays indicated that caspase-3/7 was significantly activated in a concentration-dependent manner by both piperidines, 2608 and 2610, which agrees with our results. Overall, our findings suggest that both piperidones induce the apoptosis pathway to induce cell death on both cell lines.

The DAPI staining flow cytometry protocol, to measure total cellular DNA contents, was used to examine whether 2608 and 2610 compounds could alter the cell cycle profile and reveal their potential DNA fragmentation activity on CEM and COLO 205 cell lines [14, 53–55]. Both 2608 and 2610 did not change the cell cycle profile in the two cell lines tested (Fig. 6). More specifically, 2608 induced DNA fragmentation on CEM cells but not in COLO 205 cells. In contrast, 2610 caused DNA fragmentation on both tested cell lines (Fig. 6 A). Thus, the DNA fragmentation activity of 2608 was selective on CEM cells, whereas 2610 exhibited this activity on both cell lines tested. Also, both 2608 and 2610 compounds did not induce cell cycle arrest. Cells that are undergoing apoptosis display the morphological characteristic of DNA fragmentation[43].

The ubiquitin-proteasome system has been known for the recognition and degradation of misfolded proteins in addition to performing essential roles in DNA replication, cell cycle regulation, cell migration, and immune response [56]. Prior work from our laboratory and others has demonstrated that piperidones induced proteasome inhibition [9]. Piperidone compounds P1 and P2 displayed similar polyubiquitination and increased Noxa protein expression in HL-60 cells [9]. Due to the similar structure and activity of the compounds, we investigated if the piperidones could also inhibit proteasome activity in both CEM and COLO 205. As demonstrated in previous works, piperidones have been shown to cause the accumulation of polyubiquitinated proteins [41]. Our results revealed that piperidone compound 2610 displayed a strong increase in polyubiquitinated protein accumulation in COLO 205, suggesting the inhibition of the proteome. In comparison, a fold increase was displayed more so in COLO 205 than in CEM for compound 2610. Compound 2608 displayed a moderate increase in polyubiquitinated proteins in both COLO 205 and CEM. In addition, MG 132 displayed slight proteasome inhibition in the CEM cell line in comparison to COLO 205. These data parallel our previous results with piperidones P1 and P2 in the polyubiquitination in both cell lines upon treatment with piperidones 2608 and 2610 suggesting that they also inhibit the proteasome [9]. As been previously shown, the results suggest that these piperidones induce cell death partly due to moderate inhibition of proteasome function [41]. Further

work would need to be conducted to advance the understanding of 2608 and 2610 compounds as proteasomal inhibitors. In order to further confirm that said compounds are proteasomal inhibitors, we sought to compare the compounds with piperidone b-AP15, which is a known proteasome inhibitor. Here we characterized compounds 2608 and 2610 that display structural similarity with b-AP15, which have been shown to act as inhibitors of proteasomal associated deubiquitinates (DUBs) [31, 57]. Previous work has demonstrated the ability of b-AP15 to inhibit two 19 S regulatory DUBs, UCH-L5 and USP-14 [31]. It was also shown that b-AP15 displays cytotoxicity to various cancer cell types, including multiple myeloma cells resistant to the 20 S proteasome inhibitor bortezomib, suggesting that proteasome DUB inhibitors may have clinical potential [24]. Recent studies also support the notion that deubiquitinating enzymes (DUB) are essential factors in proteolytic degradation and that their aberrant activity is linked to cancer progression and chemoresistance [57]. Here we focused primarily on the potential binding affinity of compounds 2608 and 2610 to UCH-L5 and USP-14, seeing as both compounds have a similar structure as b-AP15. With this in mind, the two compounds may also target the same DUBs as b-AP15. Our docking experiments suggested that both piperidones could interact with the same DUBs as b-AP15 and likely inhibit the proteasome similarly to the b-AP15 compound.

In summary, both piperidones were shown to possess favorable cytotoxic properties on 14 cell lines, consisting of hematological cancers and solid tumor cells, from the low nanomolar to the low micromolar range (0.009 μM to 1.664 μM). The two piperidones consistently induced cell death *via* the intrinsic apoptotic pathway, as evidenced and confirmed by the phosphatidylserine (PS) externalization, ROS generation, caspase 3/7 activation, mitochondrial depolarization, and DNA fragmentation for both CEM and COLO 205. Furthermore, the two piperidones exhibited attractive antiproliferative, cytotoxic properties and suitable action mechanisms to be considered potential anticancer drugs.

Acknowledgements The authors thank the staff of the Border Biomedical Research Center at the University of Texas at El Paso (UTEP), in particular to Ms. Gladys Almodovar, for cell culture expertise and the Cellular Characterization and Biorepository (CCB) Core Facility. Also, the authors thank the Office of the Executive Vice Chancellor for Academic Affairs, Indiana University Kokomo, USA, and the Maunders McNeil Foundation Inc., Canada, for financial support for this study.

Author contribution RMS performed most of the experiments and wrote the MS. LC performed some experiments. AVR contributed to the writing and editing as well as some experiments. MH and UD performed synthesis of compounds. CAV performed the in silico docking experiments and prepared the figures and that section of the MS. JRD supervised and created the synthetic scheme of the compounds and edited MS. MLP contributed to the conceptualization and design of the experiments and edited MS. RJA supervised all aspects of the work, wrote sections, and edited the MS. All authors read and approved the final manuscript.

Funding Funding for this work was provided by the National Institute of General Medical Sciences-Support of Competitive Research grant 1SC3GM103713-03 to RJA and the National Institutes of Health (NIH) R01CA196266 to MLP. LC and CAV were supported by the RISE Scholars Program at UTEP, funded by NIGMS grant R25GM069621-18. This work was also supported by grant 5U54MD007592 to the Border Biomedical Research Center (BBRC) at UTEP from the National Institute on Minority Health and Health Disparities, a component of the National Institutes of Health.

Data Availability The corresponding author should be contacted to request data or materials presented in this paper.

Declarations

Conflict of interest Dr. Manuel L. Penichet has a financial interest in Stellar Biosciences, Inc. The regents of the University of California are in discussions with Stellar Biosciences to license a technology invented by Dr. Penichet to this firm. In addition, Dr. Penichet has a financial interest in Klyss Biotech, Inc. All the other authors declare that the research was conducted in the absence of any commercial or financial relationships that could be construed as a potential conflict of interest. The other authors declare that they have no conflict of interest.

Ethical approval This article does not contain any studies on human participants or animals performed by any of the authors.

Informed consent For this type of study, formal consent is not required.

Competing interests The authors have declared that no competing interests exist.

References

1. Siegel RL, Miller KD, Goding Sauer A et al (2020) Colorectal cancer statistics, 2020. CA: A Cancer. J Clin 70:145–164. https://doi.org/10.3322/caac.21601
2. Siegel RL, Miller KD, Fuchs HE, Jemal A (2022) Cancer statistics, 2022. CA: A Cancer. J Clin 72:7–33. https://doi.org/10.3322/CAAC.21708
3. Barrington-Trimis JL, Cockburn M, Metayer C et al (2015) Rising rates of acute lymphoblastic leukemia in Hispanic children: Trends in incidence from 1992 to 2011. Blood 125:3033–3034
4. Das S, da Silva CJ, de Silva M et al (2018) Highly functionalized piperidines: Free radical scavenging, anticancer activity, DNA interaction and correlation with biological activity. J Adv Res 9:51–61. https://doi.org/10.1016/j.jare.2017.10.010
5. Zhou Y, Gregor VE, Ayida BK et al (2007) Synthesis and SAR of 3,5-diamino-piperidine derivatives: Novel antibacterial translation inhibitors as aminoglycoside mimetics. Bioorg Med Chem Lett 17:1206–1210. https://doi.org/10.1016/j.bmcl.2006.12.024
6. Misra M, Pandey SK, Pandey VP et al (2009) Organocatalyzed highly atom economic one pot synthesis of tetrahydropyridines as antimalarials. Bioorg Med Chem 17:625–633. https://doi.org/10.1016/j.bmc.2008.11.062
7. Rao KN, Redda KK, Onayemi FY et al (1995) Synthesis of some N-[pyridyl(phenyl)carbonylamino]hydroxyalkyl-(benzyl)-1,2,3,6-tetrahydropyridines as potential anti-inflammatory

agents. J Heterocycl Chem 32:307–315. https://doi.org/10.1002/jhet.5570320151
8. Aeluri R, Alla M, Bommena VR et al (2012) Synthesis and antiproliferative activity of polysubstituted tetrahydropyridine and piperidin-4-one-3-carboxylate derivatives. Asian J Org Chem 1:71–79. https://doi.org/10.1002/ajoc.201200010
9. Contreras L, Calderon RI, Varela-Ramirez A et al (2018) Induction of apoptosis via proteasome inhibition in leukemia/lymphoma cells by two potent piperidones. Cell Oncol 41:623–636. https://doi.org/10.1007/s13402-018-0397-1
10. Hossain M, Das S, Das U et al (2020) Novel hybrid molecules of 3,5-bis(benzylidene)-4-piperidones and dichloroacetic acid which demonstrate potent tumour-selective cytotoxicity. Bioorg Med Chem Lett 30. https://doi.org/10.1016/j.bmcl.2019.126878
11. Zhang SL, Hu X, Zhang W et al (2015) Development of pyruvate dehydrogenase kinase inhibitors in medicinal chemistry with particular emphasis as anticancer agents. Drug Discovery Today 20:1112–1119
12. Das S, Gul HI, Das U et al (2018) Novel Conjugated Unsaturated Ketones with Submicromolar Potencies Towards some Leukemic and Colon Cancer Cells. Med Chem 15:430–438. https://doi.org/10.2174/1573406414666181015142633
13. Hossain M, Das U, Dimmock JR(2019) Recent advances in α,β-unsaturated carbonyl compounds as mitochondrial toxins.European Journal of Medicinal Chemistry183
14. Robles-Escajeda E, Das U, Ortega NM et al (2016) A novel curcumin-like dienone induces apoptosis in triple-negative breast cancer cells. Cell Oncol 39:265–277. https://doi.org/10.1007/s13402-016-0272-x
15. Lema C, Varela-Ramirez A, Aguilera RJ (2011) Differential nuclear staining assay for high-throughput screening to identify cytotoxic compounds. Curr Cell Biochem 1(1):1–14
16. Robles-Escajeda E, Martínez A, Varela-Ramirez A et al (2013) Analysis of the cytotoxic effects of ruthenium-ketoconazole and ruthenium-clotrimazole complexes on cancer cells. Cell Biol Toxicol 29:431–443. https://doi.org/10.1007/s10565-013-9264-z
17. Santiago-Vázquez Y, Das U, Varela-Ramirez A et al (2016) Tumor-selective Cytotoxicity of a Novel Pentadiene Analogue on Human Leukemia/lymphoma Cells. Clin Cancer Drugs 3:138–146. https://doi.org/10.2174/2212697x03666160830165250
18. Donoso-Bustamante V, Borrego EA, Schiaffino-Bustamante Y et al (2020) An acylhydroquinone derivative produces OXPHOS uncoupling and sensitization to BH3 mimetic ABT-199 (Venetoclax) in human promyelocytic leukemia cells. Bioorg Chem 100. https://doi.org/10.1016/j.bioorg.2020.103935
19. Villanueva PJ, Martinez A, Baca ST et al (2018) Pyronaridine exerts potent cytotoxicity on human breast and hematological cancer cells through induction of apoptosis. PLoS ONE 13. https://doi.org/10.1371/journal.pone.0206467
20. Morán-Santibañez K, Vasquez AH, Varela-Ramirez A et al (2019) Larrea tridentata extract mitigates oxidative stress-induced cytotoxicity in human neuroblastoma SH-SY5Y cells. https://doi.org/10.3390/antiox8100427. Antioxidants 8:
21. Gutierrez DA, DeJesus RE, Contreras L et al (2019) A new pyridazinone exhibits potent cytotoxicity on human cancer cells via apoptosis and poly-ubiquitinated protein accumulation. Cell Biol Toxicol 35:503–519. https://doi.org/10.1007/s10565-019-09466-8
22. ECL (Enhanced Chemiluminescence) Reagents: Enhanced How? https://info.gbiosciences.com/blog/ecl-enhanced-chemiluminescence-reagents-enhanced-how. Accessed 14 Jun 2021
23. TI D, NS A, OI O et al (2018) Molecular docking analysis of phyto-constituents from Cannabis sativa with pfDHFR. Bioinformation 14:574–579. https://doi.org/10.6026/97320630014574
24. Wang X, D'Arcy P, Caulfield TR et al (2015) Synthesis and Evaluation of Derivatives of the Proteasome Deubiquitinase Inhibitor b-AP15. Chem Biol Drug Des 86:1036. https://doi.org/10.1111/CBDD.12571
25. HenrÍquez G, Mendez L, Varela-Ramirez A et al (2020) Neuroprotective Effect of Brazilin on Amyloid β (25–35)-Induced Pathology in a Human Neuroblastoma Model. ACS Omega 5:13785–13792. https://doi.org/10.1021/acsomega.0c00396
26. Robles-Escajeda E, Lerma D, Nyakeriga AM et al (2013) Searching in Mother Nature for Anti-Cancer Activity: Anti-Proliferative and Pro-Apoptotic Effect Elicited by Green Barley on Leukemia/Lymphoma Cells. PLoS ONE 8:73508. https://doi.org/10.1371/journal.pone.0073508
27. Redza-Dutordoir M, Averill-Bates DA (2016) Activation of apoptosis signalling pathways by reactive oxygen species. Biochimica et Biophysica Acta (BBA) -. Mol Cell Res 1863:2977–2992. https://doi.org/10.1016/J.BBAMCR.2016.09.012
28. Suski JM, Lebiedzinska M, Bonora M et al (2012) Relation between mitochondrial membrane potential and ROS formation. Methods Mol Biol 810:183–205. https://doi.org/10.1007/978-1-61779-382-0_12
29. Torres-Roca JF, Lecoeur H, Amatore C, Gougeon ML (1995) The early intracellular production of a reactive oxygen intermediate mediates apoptosis in dexamethasone-treated thymocytes. Cell Death Differ 2(4):309–319
30. Degterev A, Boyce M, Yuan J (2003) A decade of caspases. Oncogene 22:8543–8567
31. D'Arcy P, Brnjic S, Olofsson MH et al (2011) Inhibition of proteasome deubiquitinating activity as a new cancer therapy. Nat Med 17:1636–1640. https://doi.org/10.1038/nm.2536
32. Mujtaba T, Dou QP (2011) Advances in the Understanding of Mechanisms and Therapeutic Use of Bortezomib. Discov Med 12:471–480
33. Lam YA, Xu W, DeMartino GN, Cohen RE(1997) Editing of ubiquitin conjugates by an isopeptidase in the 26S proteasome. Nature 1997 385:6618 385:737–740. https://doi.org/10.1038/385737a0
34. Yao T, Cohen RE(2002) A cryptic protease couples deubiquitination and degradation by the proteasome. Nature 2002 419:6905 419:403–407. https://doi.org/10.1038/nature01071
35. Leggett DS, Hanna J, Borodovsky A et al (2002) Multiple Associated Proteins Regulate Proteasome Structure and Function. Mol Cell 10:495–507. https://doi.org/10.1016/S1097-2765(02)00638-X
36. Borodovsky A, Kessler BM, Casagrande R et al (2001) A novel active site-directed probe specific for deubiquitylating enzymes reveals proteasome association of USP14. EMBO J 20:5187. https://doi.org/10.1093/EMBOJ/20.18.5187
37. Kish-Trier E, Hill CP (2013) Structural Biology of the Proteasome. Annu Rev Biophys 42:29. https://doi.org/10.1146/ANNUREV-BIOPHYS-083012-130417
38. Tomko RJ Jr, Hochstrasser M (2013) Molecular Architecture and Assembly of the Eukaryotic Proteasome. Annu Rev Biochem 82:415–445. https://doi.org/10.1146/ANNUREV-BIOCHEM-060410-150257
39. Chadchankar J, Korboukh V, Conway LC et al (2019) Inactive USP14 and inactive UCHL5 cause accumulation of distinct ubiquitinated proteins in mammalian cells. PLoS ONE 14. https://doi.org/10.1371/JOURNAL.PONE.0225145
40. Das U, Alcorn J, Shrivastav A et al (2007) Design, synthesis and cytotoxic properties of novel 1-[4-(2-alkylaminoethoxy) phenylcarbonyl]-3,5-bis(arylidene)-4-piperidones and related compounds. Eur J Med Chem 42:71–80. https://doi.org/10.1016/J.EJMECH.2006.08.002
41. Contreras L, Medina S, Schiaffino Bustamante AY et al (2022) Three novel piperidones exhibit tumor-selective cytotoxicity on leukemia cells via protein degradation and stress-mediated mechanisms. Pharmacol Rep 74:159. https://doi.org/10.1007/S43440-021-00322-3

42. Varela-Ramirez A, Costanzo M, Carrasco YP et al (2011) Cytotoxic effects of two organotin compounds and their mode of inflicting cell death on four mammalian cancer cells. Cell Biol Toxicol 27:159–168. https://doi.org/10.1007/s10565-010-9178-y
43. Alberts B, Johnson A, Lewis J et al (2002) Molecular Biology of the Cell. Programmed Cell Death (Apoptosis). Garland Science
44. Carneiro BA, El-Deiry WS (2020) Targeting apoptosis in cancer therapy. Nat Rev Clin Oncol 17:395. https://doi.org/10.1038/S41571-020-0341-Y
45. Fulda S, Debatin KM (2006) Extrinsic versus intrinsic apoptosis pathways in anticancer chemotherapy. Oncogene 25:4798–4811
46. Kroemer G, Galluzzi L, Brenner C (2007) Mitochondrial membrane permeabilization in cell death. Physiol Rev 87:99–163. https://doi.org/10.1152/PHYSREV.00013.2006/ASSET/IMAGES/LARGE/Z9J0010724230012.JPEG
47. Wu CC, Bratton SB (2013) Regulation of the intrinsic apoptosis pathway by reactive oxygen species. Antioxid Redox Signal 19:546–558
48. Loeffler M, Kroemer G (2000) The mitochondrion in cell death control: Certainties and incognita. Exp Cell Res 256:19–26. https://doi.org/10.1006/excr.2000.4833
49. Henderson CJ, Aleo E, Fontanini A et al (2005) Caspase activation and apoptosis in response to proteasome inhibitors. Cell Death Differ 12:1240–1254. https://doi.org/10.1038/sj.cdd.4401729
50. Li H, Zhu H, Xu CJ, Yuan J (1998) Cleavage of BID by caspase 8 mediates the mitochondrial damage in the Fas pathway of apoptosis. Cell 94:491–501. https://doi.org/10.1016/S0092-8674(00)81590-1
51. Lund T, Stokke T, Olsen E, Fodstad (2005) Garlic arrests MDA-MB-435 cancer cells in mitosis, phosphorylates the proapoptotic BH3-only protein BimEL and induces apoptosis. Br J Cancer 92:1773–1781. https://doi.org/10.1038/sj.bjc.6602537
52. Ferguson PJ, Kurowska E, Freeman DJ et al (2004) A flavonoid fraction from cranberry extract inhibits proliferation of human tumor cell lines. J Nutr 134:1529–1535. https://doi.org/10.1093/JN/134.6.1529
53. Nakamura-Bencomo S, Gutierrez DA, Robles-Escajeda E et al (2021) Recombinant human lactoferrin carrying humanized glycosylation exhibits antileukemia selective cytotoxicity, microfilament disruption, cell cycle arrest, and apoptosis activities. Investig New Drugs 39:400–415. https://doi.org/10.1007/S10637-020-01020-2/FIGURES/8
54. Gutierrez DA, Contreras L, Villanueva PJ et al (2022) Identification of a Potent Cytotoxic Pyrazole with Anti-Breast Cancer Activity That Alters Multiple Pathways. Cells 11:254. https://doi.org/10.3390/CELLS11020254/S1
55. Donoso-Bustamante V, Borrego EA, Schiaffino-Bustamante Y et al (2020) An acylhydroquinone derivative produces OXPHOS uncoupling and sensitization to BH3 mimetic ABT-199 (Venetoclax) in human promyelocytic leukemia cells. Bioorg Chem 100:103935. https://doi.org/10.1016/J.BIOORG.2020.103935
56. Melvin AT, Woss GS, Park JH et al (2013) Measuring Activity in the Ubiquitin-Proteasome System: From Large Scale Discoveries to Single Cells Analysis. Cell Biochem Biophys 67:75–89. https://doi.org/10.1007/s12013-013-9621-9
57. Coughlin K, Anchoori R, Iizuka Y et al (2014) Small-Molecule RA-9 Inhibits Proteasome-Associated DUBs and Ovarian Cancer In Vitro and In Vivo via Exacerbating Unfolded Protein Responses. Clin Cancer Res 20:3174–3186. https://doi.org/10.1158/1078-0432.CCR-13-2658